Hydrogen elimination model of the formation of hydrogen bonding structures during the growth of hydrogenated amorphous silicon by plasma CVD

Akira Terakawa*
Department of Electronic Science and Engineering, Kyoto University, Yoshidahonmachi, Sakyo, Kyoto 606-8501, Japan and New Materials Research Center, Sanyo Electric Co., Ltd., 1-1 Dainichi Higashimachi, Moriguchi, Osaka 570-8502, Japan

Hiroyuki Matsunami
Department of Electronic Science and Engineering, Kyoto University, Yoshidahonmachi, Sakyo, Kyoto 606-8501, Japan
(Received 27 January 2000)

The correlations between the [dihydride]/[monohydride] ratio and the H content in hydrogenated amorphous silicon (a-Si:H) and alloy materials were studied statistically for data obtained from infrared absorption spectroscopy. A hydrogen-elimination (HE) model, which is based on the thermally activated elimination of H atoms from SiH_3 precursors, is proposed to describe the formation kinetics of H-Si bonding configurations during film growth. The experimental results were compared with a continuous random network (CRN) model and the HE model. It was found that a-Si:H deposited using a low rf power and a low H_2-dilution SiH_4 plasma selectively contains Si-H_2 structures, while a high H_2-dilution method reduces Si-H_2 resulting in an almost random network. The selective Si-H_2 formation is probably caused by the larger activation energy for H-elimination from Si-H_2 rather than from Si-H. It is proposed that the H_2-dilution effects activate the H-elimination and reconstruction of the network, and decrease Si-H_2 to maximize the entropy of the arrangement of H atoms. The HE model can quantitatively describe the deposition condition dependence of the H bonding structures. Furthermore, it was suggested that the random H-elimination reactions can cause selective Si-H formation compared to the CRN model.

I. INTRODUCTION

Hydrogenated amorphous silicon (a-Si:H) and its alloy materials deposited by plasma chemical vapor deposition (CVD) methods are important for large-area semiconductor devices, such as solar cells. A stabilized efficiency of 9.5% for a submodule (1200 cm^2) with an a-Si/a-SiGe tandem cell structure, the world's highest, was recently achieved.[1] Incorporated H atoms and H-Si bonding structures in the materials play a dominant role in determining the optoelectronic properties. A study of the stretching vibrational modes of H-Si bonding from infrared (IR) absorption spectra provides information about the H bonding configurations. The absorption peak located at $\sim$2000 cm^{-1} is associated with monohydride (Si-H) structures, and that located at $\sim$2100 cm^{-1} is associated with dihydride (Si-H_2) or clustered void structures.[2,3] It has often been reported that an increase in the Si-H_2 concentration cause a deterioration in photoconductivity, increased defect density and poorer photostability.[4–10] In order to control material quality, it is essential to control the H bonding configurations. Therefore, it is of interest to clarify the formation mechanism of H bonding structures during deposition.

Hydrogen content, C_H, is a factor affecting the H bonding structures in the a-Si:H network. When C_H increases, the probability of a certain Si atom bonding to multiple H atoms increases and more polyhydride structures seem to appear. Many research groups have previously reported 1-to-1 positive correlations between the Si-H_2 content and C_H for a-Si:H deposited by various deposition systems such as plasma CVD or magnetron sputtering methods.[6,11–14] Some research groups have tried to explain these correlations by statistical considerations based on random models of H and Si atoms in the a-Si:H network, and have succeeded in qualitatively explaining the increase in the Si-H_2 content with C_H.[11,14] However, it has been reported that the use of deposition techniques, such as highly H_2-diluted SiH_4 plasma or post H-plasma treatment, can reduce the Si-H_2 content independent of C_H.[6,10] Hence, the previous random models, which do not take into account the deposition mechanism, could not explain the changes in the bonding structures that depend on the process conditions.

The kinetics of a-Si:H growth is considered to be as follows. SiH_3* and H* radicals generated in the plasma impinge on and stick to the growing surface. The topmost layer of a growing film is covered by Si-H_3 structures, and the $C_H(=[H]/[Si])$ of this region is $\sim$300 at%. During the growth of several atomic layers, excess H atoms are released and the C_H reaches the steady state value of the bulk at 10–20 at%. Ganguly and Matsuda have proposed a surface diffusion (SD) model to describe the relationship between a-Si:H film properties and the process conditions of plasma CVD. The model assumed that the defect density in the film bulk is simply determined by the defect density at the top of the growing film.[15] Although the SD model explains the relationship among the defect density, growth rate and process temperature, it does not quite come to grips with the formation of H bonding configurations in the growth zone. Maeda *et al.* have considered the process condition dependence of the H bonding structures.[16] They assumed two H-elimination reactions with different rates, and tried to explain the increase in Si-H_2 with an increase in the growth rate. Even

0163-1829/2000/62(24)/16808(7)/$15.00 ©2000 The American Physical Society

TABLE I. Deposition conditions of samples.

Substrate temperature	80–350 °C
Reaction pressure	~20 Pa
Background pressure	10^{-5}–10^{-6} Pa
RF power density	20–300 mW/cm^2
Hydrogen dilution ratio	0–30 for a-Si:H
$[H_2]/([GeH_4]+[SiH_4])$	2.5–40 for a-SiGe:H

their model could not quantitatively describe the H bonding configurations in the a-Si:H network. Some *ab initio* approaches have also been carried out. Sato *et al.*, Nakajima *et al.*, and Srinivasan *et al.* have reported the configuration dependence of the activation energy for H-elimination reactions.[17–20] However, the scale of the *ab initio* calculations is limited to only several Si-atom clusters at the present stage, and it has not yet been possible to apply the method to a large-scale a-Si:H network.

In this paper, a new statistical model is proposed to quantitatively describe the deposition condition dependence of the H bonding structures in a-Si:H, by simulating the thermally activated H-elimination reactions in the growth zone. The C_H dependence of the network structures using a H-elimination (HE) model is compared with the experimental results of IR absorption analysis and a continuous random network (CRN) model. The effect of H_2-dilution techniques on the H bonding structures is also discussed.

II. HYDROGEN BONDING STRUCTURES

A. IR analysis of a-Si:H and a-SiGe:H

a-Si:H and a-SiGe:H films with a thickness of 0.2–1.0 μm were deposited in an rf plasma-CVD reactor. The deposition conditions are shown in Table I. The IR absorption spectra were decomposed of two (for a-Si:H) or three (for a-SiGe:H) Gaussian curves centered at frequencies of ~1860, ~2000, and ~2100 cm^{-1}, which were assigned to the stretched vibrational modes of Ge–H, Si-H, and Si-H_2, respectively. The H content (C_H) was defined as $[H]/([Si]+[Ge])$. The bonded H content in each configuration $[C_H(\text{Ge-H}), C_H(\text{Si-H}), \text{and } C_H(\text{Si-H}_2)]$ was evaluated by distributing the C_H proportional to the product of the calibration factor (A_{Si} or A_{Ge}) and the area under the Gaussian curve of each mode.[12] The details of the experimental procedure are presented elsewhere.[9,21]

Figure 1 shows the $C_H(\text{Si-H}_2)/C_H(\text{Si-H})$ of a-Si:H ($R_{a\text{-Si:H}}$) deposited from low-dilution ($[H_2]/[SiH_4]<2.5$) and high-dilution ($[H_2]/[SiH_4]>10$) source gases plotted against C_H. The $R_{a\text{-Si:H}}$ for the low-dilution a-Si:H samples has a 1-to-1 correlation to C_H, as previously reported.[6,11–14] The $R_{a\text{-Si:H}}$ ratio can be reduced independent of C_H by the use of high dilution. Figure 2 shows the $C_H(\text{Si-H}_2)/C_H(\text{Si-H})$ of a-SiGe:H ($R_{a\text{-SiGe:H}}$) deposited from low-dilution ($[H_2]/([SiH_4]+[GeH_4])=2.5$) and high-dilution ($[H_2]/([SiH_4]+[GeH_4])=20$–$40$) mixture gases as a function of the content of bonded H to Si, $C_H(\text{Si})$ $(=(C_H(\text{Si-H}_2)+C_H(\text{Si-H}))/C_{Si})$. The broken line in Fig. 2 indicates the $R_{a\text{-Si:H}}$-C_H trend for low-dilution a-Si:H replotted from Fig. 1. The $R_{a\text{-SiGe:H}}$-$C_H(\text{Si})$ correlation for low-dilution a-SiGe:H is similar to the $R_{a\text{-Si:H}}$-C_H correlation for

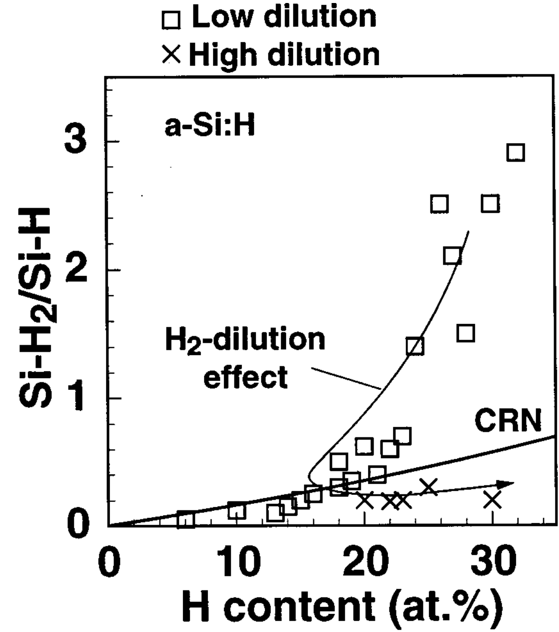

FIG. 1. [dihydride]/[monohydride] ratio for a-Si:H samples ($R_{a\text{-Si:H}}=C_H(\text{Si-H}_2)/C_H(\text{Si-H})$) plotted against H content (C_H) deposited from low dilution ($[H2]/[SiH4]<2.5$) and high dilution ($[H_2]/[SiH_4]>10$) source gases. The arrow indicates a schematic trend for increasing H_2-dilution ratios (H_2-dilution effects). The solid line indicates the trend of the continuous random network (CRN) model for a-Si:H represented in Eq. (9).

a-Si:H. In addition, the $R_{a\text{-SiGe:H}}$ can be reduced by a high H_2-dilution source gas as was the case for a-Si:H. The $R_{a\text{-SiGe:H}}$-$C_H(\text{Si})$ correlations for both low- and high-dilution a-SiGe:H samples (Fig. 2) are similar to the $R_{a\text{-Si:H}}$-C_H correlations in a-Si:H (Fig. 1). This suggests that there exists a common mechanism determining the H-Si bonding structures in both a-Si:H and a-SiGe:H.[21]

B. Continuous random network (CRN) model

Continuous random network (CRN) models[22] have been considered useful for describing the amorphous network, because nonequilibrium amorphous structures seem to correspond to the maximum entropy of atomic arrangement. In this section, H-Si bonding structures in a CRN are considered, on the assumption that Si and H atoms are randomly mixed. The CRN is assumed to be composed of M four-valent Si atoms and L mono-valent H atoms. All H atoms combine with Si atoms, and the number of dangling bonds is negligible compared to M and L. The number of H-Si bonds, $N_{\text{H-Si}}$, and Si-Si bonds, $N_{\text{Si-Si}}$, can be represented as

$$N_{\text{H-Si}}=L=MC_H, \tag{1}$$

$$N_{\text{Si-Si}}=(4M-L)/2=M(4-C_H)/2, \tag{2}$$

where $C_H=[H]/[Si]=L/M$. The probability of a bond, sampled from the network at random, being a Si-Si bond, $p_{\text{Si-Si}}$, or a H-Si bond, $p_{\text{H-Si}}$, is represented as follows, respectively,

$$p_{\text{Si-Si}}=N_{\text{Si-Si}}/(N_{\text{H-Si}}+N_{\text{Si-Si}})=(4-C_H)/(4+C_H), \tag{3}$$

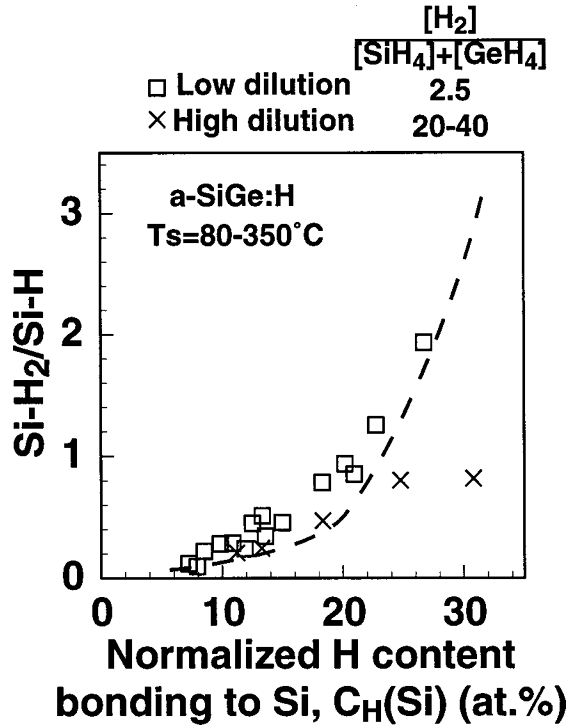

FIG. 2. [dihydride]/[monohydride] ratio for a-SiGe:H samples ($R_{a\text{-SiGe:H}} = C_H(\text{Si-H}_2)/C_H(\text{Si-H})$) plotted against H content bonded to Si ($C_H(\text{Si})$) deposited from low-dilution ($[H_2]/([SiH_4]+[GeH_4])=2.5$) and high-dilution ($[H_2]/([SiH_4]+[GeH_4])=20-40$) source gases. The broken line indicates the trend for low dilution a-Si:H samples.

$$p_{\text{H-Si}} = 1 - p_{\text{Si-Si}} = 1 - N_{\text{Si-Si}}/(N_{\text{H-Si}} + N_{\text{Si-Si}}) = 2C_H/(4+C_H). \tag{4}$$

When a H atom is sampled from the network at random, the probability of the configuration of the H-Si bond being the monohydride—in other words, the remaining three valences of the Si atom connected with the neighboring Si—is $p^3_{\text{Si-Si}}$. By a similar consideration, the H content in different configurations can be represented as

$$C_H(\text{Si-H}) = C_H p^3_{\text{Si-Si}} = C_H(4-C_H)^3/(4+C_H)^3, \tag{5}$$

$$C_H(\text{Si-H}_2) = 3C_H p_{\text{H-Si}} p^2_{\text{Si-Si}} = 6C_H^2(4-C_H)^2/(4+C_H)^3, \tag{6}$$

$$C_H(\text{Si-H}_3) = 3C_H p^2_{\text{H-Si}} p_{\text{Si-Si}} = 12C_H^3(4-C_H)/(4+C_H)^3, \tag{7}$$

$$C_H(\text{Si-H}_4) = C_H p^3_{\text{H-Si}} = 8C_H^4/(4+C_H)^3, \tag{8}$$

where the factor of 3 in Eqs. (6) and (7) was obtained by considering the possible number of atomic arrangements for $Si\text{-}H_2$ or $Si\text{-}H_3$ configurations. Figures 3(a) and 3(b) show the H content of SiH_n ($n=1$, 2, 3, and 4) configurations in the CRN model plotted against the H content described in Eqs. (5)–(8). Figure 3(b) shows details of the behavior in the range of $C_H = 0-30$ at % which can be compared to the bulk data shown in Figs. 1 and 2. The [polyhydride]/[monohydride] ratio of the CRN can be represented as a function of C_H as follows:

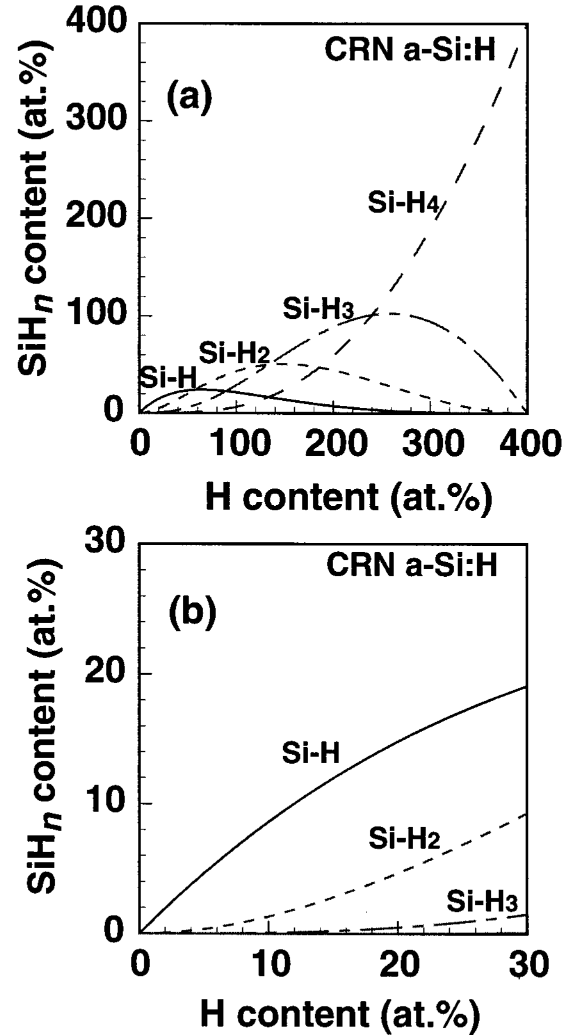

FIG. 3. Hydrogen content in SiH_n ($n=1$, 2, 3, and 4) configurations of the CRN model plotted against the H content described in Eqs. (5)–(8): (a) $C_H = 0-400$ at %, (b) $C_H = 0-30$ at % (corresponding to bulk a-Si:H).

$$\{C_H(\text{Si-H}_2) + C_H(\text{Si-H}_3) + C_H(\text{Si-H}_4)\}/C_H(\text{Si-H}) = (1-p^3_{\text{Si-Si}})/p^3_{\text{Si-Si}} = 2C_H(C_H^2+48)/(4-C_H)^3. \tag{9}$$

The solid line in Fig. 1 shows the result of the CRN model described in Eq. (9), which is quantitatively consistent with the results of a statistical computer simulation described in Ref. 14. Although the CRN model can explain the positive dependence of the $C_H(\text{Si-H}_2)/C_H(\text{Si-H})$ ratio on C_H, there is a great quantitative disagreement between the model and the experimental results of low-dilution a-Si:H. One can see that the low-dilution samples selectively contain polyhydride bonds, while the high-dilution samples approximately correspond to the CRN model. The CRN model could not describe the deposition condition dependence of H bonding configurations, either. This is because the randomness is only evident for materials fabricated by rapid cooling from the liquid phase. The process temperature during a-Si:H deposition by plasma CVD, which is at most ~300 °C, is much

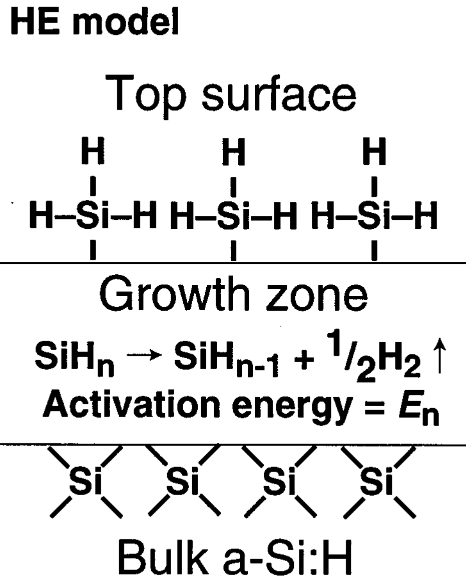

FIG. 4. A schematic illustration of the H-elimination (HE) model for a-Si:H film growth. The top surface is covered by Si-H_3 structures. Bulk a-Si:H structures are formed via H-elimination reactions in the growth zone represented by Eq. (10).

lower than the melting point of Si (~1412 °C). Under these nonequilibrium conditions, attention should be paid to another factor, the ''deposition mechanism,'' for a quantitative comprehension of H microstructures.

III. HYDROGEN ELIMINATION (HE) MODEL

A. Deposition mechanism

In order to explain the process dependence of H bonding structures, the deposition kinetics of a-Si:H has to be taken into account. The CRN model assumes the random insertion of H into the Si network or the random mixing of Si and H atoms, as mentioned before. However, in the case of deposition from low-dilution or low rf-power SiH_4 plasma, in which the effects of ion bombardment are negligible, the dominant reaction in the growing surface is the elimination of excess H atoms. In this section, we propose a new numerical model simulating the H-elimination reactions in the growth zone to analytically describe the formation mechanism of H bonding structures.

B. Numerical model

Figure 4 schematically illustrates the growth process of a-Si:H film. It was assumed that (a) the top of the growing film is covered by SiH_3 and each Si atom bonds to three H atoms, and (b) the H-Si bonding configurations in the bulk are determined simply by the H-elimination reactions. Possible H-elimination reactions and corresponding reaction rates (r_n) can be represented as follows:

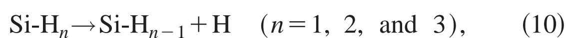

$$\text{Si-H}_n \rightarrow \text{Si-H}_{n-1} + \text{H} \quad (n=1,\ 2,\ \text{and}\ 3), \tag{10}$$

$$r_n \propto \exp(-E_n/kT) \quad (n=1,\ 2,\ \text{and}\ 3), \tag{11}$$

where E_n is an activation energy for the H-elimination from Si-H_n configurations, and k and T are the Boltzmann constant and process temperature, respectively. The change of Si-H_n content (s_n) with a very small amount of H-elimination ($\Delta C_{\text{H}} = s_1 + s_2 + s_3$) can be described as follows:

$$s_1\text{Si-H} + s_2\text{Si-H}_2 + s_3\text{Si-H}_3 \rightarrow s_1\text{Si} + s_2\text{Si-H} + s_3\text{Si-H}_2 + (s_1+s_2+s_3)\text{H} \quad (n=1,\ 2,\ \text{and}\ 3), \tag{12}$$

where s_n is proportional to both the H-elimination reaction rates (r_n) and the H content in Si-H_n configurations, and can be represented as

$$s_n \propto r_n n[\text{Si-H}_n] \propto r_n C_{\text{H}}(\text{Si-H}_n), \tag{13}$$

where [Si-H_n] indicates the density of Si-H_n structures. The H-elimination reactions shown in Eq. (12) imply s_n of Si-H_n [which corresponds to ns_n of C_{H}(Si-H_n)] is removed while s_n of Si-H_{n-1} [which corresponds to $(n-1)s_n$ of C_{H}(Si-H_{n-1})] is created simultaneously. Therefore, the decreasing ratios of C_{H}(Si-H_n) ($n=1$, 2, and 3) against decreasing C_{H} ($-\Delta C_{\text{H}}$) can be represented as follows, respectively,

$$dC_{\text{H}}(\text{Si-H}_3)/dC_{\text{H}} = 3s_3/(s_1+s_2+s_3), \tag{14}$$

$$dC_{\text{H}}(\text{Si-H}_2)dC_{\text{H}} = 2s_2/(s_1+s_2+s_3) - 2s_3/(s_1+s_2+s_3), \tag{15}$$

$$dC_{\text{H}}(\text{Si-H})/dC_{\text{H}} = s_1/(s_1+s_2+s_3) - s_2/(s_1+s_2+s_3). \tag{16}$$

According to the deposition model described in Fig. 4, the topmost layer of the growing film is covered by SiH_3 radicals. Thus, the boundary conditions at $C_{\text{H}}=3$ can be represented as follows:

$$C_{\text{H}}(\text{Si-H}) = C_{\text{H}}(\text{Si-H}_2) = 0 \quad \text{and} \quad C_{\text{H}}(\text{Si-H}_3) = 3. \tag{17}$$

It has been reported that the activation energies of H-elimination reactions during a-Si:H growth are much lower than that of simple H-Si detachment reactions.[23] This is probably because the main H-elimination reactions in a growth zone happen together with H-Si or H-H formation reactions. Equation (10) can include these multiple reactions by taking into consideration the difference in the activation energies among these reactions, although Eq. (10) indicates simple H-elimination as atomic H.

C. Analysis procedure

1. E_n = const

If E_n is independent of the H bonding configurations, H atoms eliminate randomly and r_n is constant. In the case of this random H-elimination (RHE) model, the simultaneous differential equations, Eqs. (14)–(16), can be solved under the boundary conditions, Eq. (17). The solutions become as follows:

$$C_{\text{H}}(\text{Si-H}_3) = C_{\text{H}}^3/9, \tag{18}$$

$$C_{\text{H}}(\text{Si-H}_2) = -2C_{\text{H}}^2(C_{\text{H}}-3)/9, \tag{19}$$

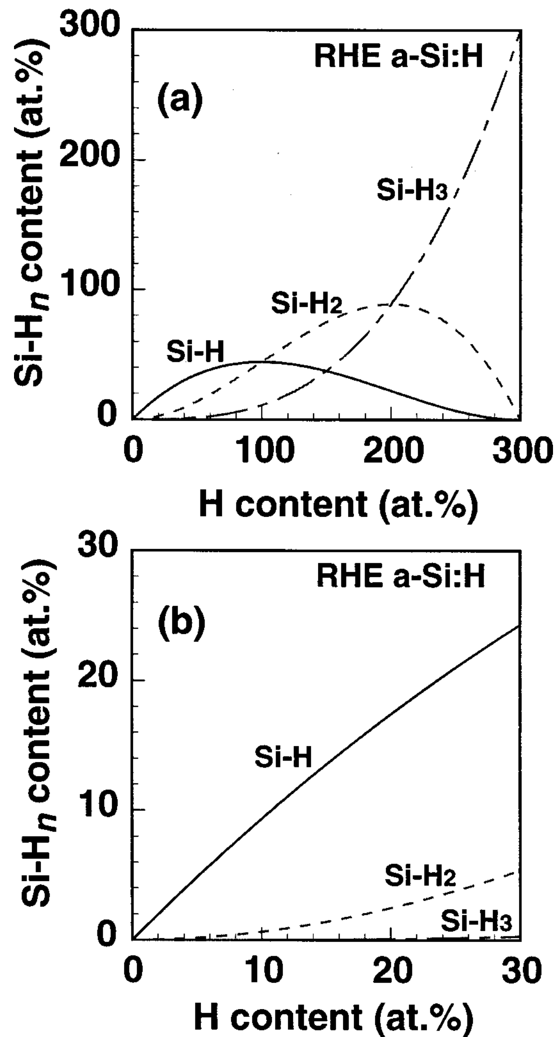

FIG. 5. Hydrogen content in SiH_n ($n=1$, 2, and 3) configurations of the random H-elimination (RHE) model plotted against the H content described in Eqs. (18)–(20): (a) $C_H=0-300$ at % (corresponding to the growth zone), (b) $C_H=0-30$ at % (corresponding to bulk a-Si:H).

$$C_H(\text{Si-H})=C_H(C_H-3)^2/9. \tag{20}$$

The solutions, Eqs. (18)–(20), are independent of T, because the r_n's in the numerators and denominators of Eqs. (14)–(16) cancel out. Figure 5(a) shows the H content of SiH_n ($n=1$, 2, and 3) configurations in the RHE model plotted against the H content described in Eqs. (18)–(20). This figure corresponds to the changing stages of the H bonding configurations—from SiH_3 radicals to the bulk— in the growth zone during deposition. Figure 5(b) shows the details in the range of $C_H=0-30$ at % to compare with the bulk data shown in Figs. 1 and 2. One can see that the polyhydride content of the RHE model is lower than that of the CRN model shown in Figs. 3(a) and 3(b) for the entire C_H region. For the RHE model, the [polyhydride]/[monohydride] ratio can be represented as a function of C_H as follows:

$$\{C_H(\text{Si-H}_3)+C_H(\text{Si-H}_2)\}/C_H(\text{Si-H}) = -C_H(C_H-6)/(C_H-3)^2. \tag{21}$$

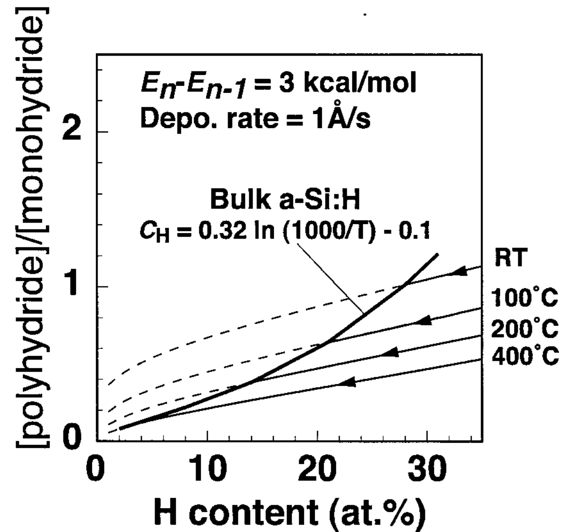

FIG. 6. [polyhydride]/[monohydride] ratio $[(C_H(\text{Si-H}_3)+C_H(\text{Si-H}_2))/C_H(\text{Si-H})]$ of the H-elimination (HE) model plotted against H content. The arrows and dashed lines indicate the stages of the H-elimination reactions and their extensions during film growth at various process temperatures, which are obtained from Eqs. (14)–(16). The bold line indicates the H bonding configurations in bulk a-Si:H, respectively, which was obtained by connecting the end points of the H-elimination reactions (corresponding to the H content in Fig. 7) for various process temperatures. Where, $E_n-E_{n-1}=3$ kcal/mol and the deposition rate of 1 Å/s were assumed.

2. $E_n \neq$ const

In the case of the RHE model (E_n=const), Eqs. (14)–(16) were solved analytically. However, E_n and r_n are generally considered to vary with the H bonding configurations. Sato *et al.*[18] and Srinivasan *et al.*[20] have each pointed out that, based on *ab initio* simulations, the rates of H desorption reactions are considered to depend on the network around the H-Si bonds. It was predicted that the activation energy of H elimination from monohydride ($E_1=7.2$ kcal/mol) is smaller than that from dihydride ($E_2=8.2-10.8$ kcal/mol), based on the assumption of H-abstraction reactions mediated through H_2-molecular formation.[20]

In the case in which the H-elimination rate is dependent on the H bonding configurations, the solutions become more complicated because they are functions of T. We solved the simultaneous differential equations, Eqs. (14)–(16), by using computer analysis (Mathematica 2.2.2 for Macintosh by Wolfram Research, Inc. was used). Figure 6 shows the [polyhydride]/[monohydride] ratios of the HE model plotted against C_H. The arrows and dashed lines indicate the changing stages of the [polyhydride]/[monohydride] ratios during H-elimination reactions for various process temperatures, which are the solutions of Eqs. (14)–(16), where, $E_n-E_{n-1}=3$ kcal/mol was assumed although $E_2-E_1=1.0-3.6$ kcal/mol in Ref. 20. The stages are strongly dependent on the process temperature, in contrast to the case of the constant E_n shown in Eqs. (18)–(21).

Now let us turn to the correlation between C_H and T. Figure 7 shows the C_H of a-Si:H deposited with ~1 and ~3

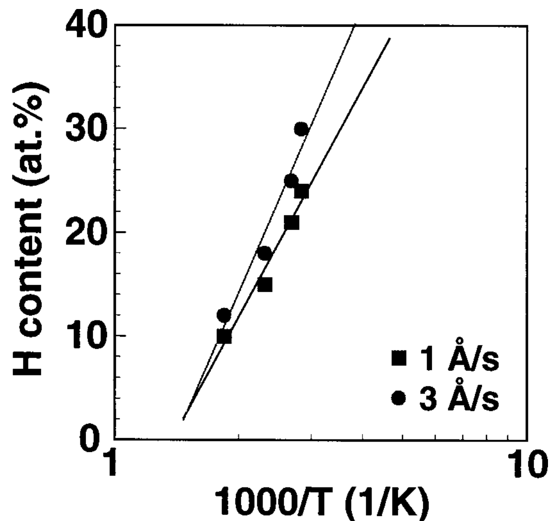

FIG. 7. Arrhenius plots of the H content of a-Si:H samples deposited with growth rates of 1 and 3 Å/s.

Å/s of growth rate plotted against the process temperature. Since the H-eliminations are thermally activated reactions, C_{H} is mainly determined by T despite the slight dependence on the deposition rate. The following empirical relation was obtained by a curve fitting of the plotted data in Fig. 7,

$$C_{\mathrm{H}}=a\ \ln(1000/T)-b, \tag{22}$$

where a and b are 0.32 and 0.10 for 1 Å/s, and 0.40 and 0.14 for 3 Å/s, respectively. Therefore,

$$T=1000/\exp\{(C_{\mathrm{H}}+b)/a\}. \tag{23}$$

By substituting Eq. (23) for T in the solutions of Eqs. (14)–(16), the end point of the H-elimination reactions in the growth zone can be determined for each temperature. The solid line in Fig. 6, which was obtained by connecting the end points of the H-elimination reactions, indicates the [polyhydride]/[monohydride] ratio in the bulk a-Si:H as a function of C_{H}.

IV. DISCUSSION

Figure 8 shows the [polyhydride]/[monohydride] ratios of the HE ($E_n-E_{n-1}=3$ kcal) and RHE ($E_n=$const) models plotted against C_{H}. The dark and bright hatched regions indicate the experimental results of the high- and low-dilution a-Si:H samples, respectively, shown in Fig. 1. The broken line in Fig. 8 shows the results of the CRN model described in Eq. (9).

Both HE and RHE models also exhibit positive dependencies on C_{H}. Although this is qualitatively similar to the CRN model, quantitative differences exist. Over the entire C_{H} region, the [polyhydride]/[monohydride] ratio of the HE model is about 2 times larger than that of the CRN model, while that of the RHE model is less than half that of the CRN model.

On the one hand, the HE model is closer to the trend of the low-dilution samples than the RHE or CRN models. The preferential Si-H_2 formation in the low-dilution a-Si:H is caused by the selective H desorption from monohydride structures due to the smaller activation energy, as mentioned

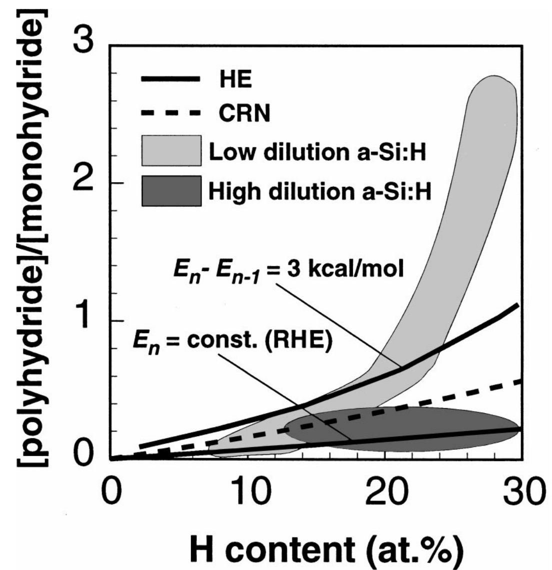

FIG. 8. A comparison of the [polyhydride]/[monohydride] ratio $[(C_{\mathrm{H}}(\text{Si-H}_3)+C_{\mathrm{H}}(\text{Si-H}_2))/C_{\mathrm{H}}(\text{Si-H})]$ among HE ($E_n-E_{n-1}=3$ kcal/mol) and RHE ($E_n=$const) models plotted against C_{H}. The dark and bright hatched regions indicate the IR experimental results of the high- and low-dilution a-Si:H samples, respectively, as shown in Fig. 1. The broken line indicates the CRN model represented in Eq. (9).

before. However, in the high-C_{H} region (>25 at %) larger [polyhydride]/[monohydride] ratio than the HE model predicts cannot be explained for reasonable differences between the activation energies for the different configurations. The excess SiH_2 signal in the IR experiments probably originates from H-Si bonds in the internal surface of voids or $(SiH_2)_n$ chain structures due to suppressed surface reactions at the low temperature. On the other hand, the RHE model approximately agrees with the trend of the high-dilution samples. In the case of the high H_2-dilution process, abundant H* radicals supplied from the plasma might reduce the activation energies for H-elimination from polyhydrides and hence enhance the H-elimination reactions. In addition, the high-dilution deposition processes are thought to supply enough energy to cause H-elimination and insertion reactions by H radicals or ions impinging on the surface. These reactions cause an active reconstruction of amorphous network, and result in random H-bonding configurations which give the largest entropy for the arrangement of H atoms.

One can see that the RHE model causes fewer polyhydride structures than the CRN model in the region with C_{H} less than 30 at %. It is expected that the random H-elimination reactions for appropriate H_2-dilution conditions can result in selective monohydride structures, leading to improvements in both the electronic properties and the photostability of materials.

It is possible that the eliminated H recombines with Si again in the growth zone. Under high growth-rate and/or low H-elimination-rate conditions, the effects of buried H atoms seem to be remarkable. If buried H atoms recombine with Si atoms randomly, the H bonding configurations may be expected to depart from the HE model and approach the CRN model. As a result the SiH_2/SiH ratio should decrease (Fig. 8). However, contrary to the expectation, it has been reported for a-Si:H deposited from nondiluted SiH_4 plasmas

that SiH_2/SiH ratios increase under process conditions with low temperatures and high growth rates.[6] Buried H atoms are considered to be captured in hydrogen rich regions selectively, and form H clusters or polyhydride structures.

V. CONCLUSIONS

The correlations between the [polyhydride]/[monohydride] ratio and the H content (C_H) in hydrogenated *a*-Si:H and *a*-SiGe:H were studied statistically. The experimental results of an infrared (IR) absorption analysis were compared with a continuous random network (CRN) model and a H-elimination (HE) model. The conclusions are summarized below.

(1) *a*-Si:H deposited from the low H_2-dilution plasma selectively contains Si-H_2 structures, while a high H_2-dilution method reduces Si-H_2 resulting in an almost random *a*-Si network. The selective Si-H_2 formation is explainable by the larger activation energy for H-elimination from Si-H_2 rather than from Si-H. It is supposed that the H_2-dilution effects activate the H-elimination and reconstruction of the network, and decrease Si-H_2 to maximize the entropy for the arrangement of H atoms.

(2) Both the CRN and HE models can represent the positive correlations between the [polyhydride]/[monohydride] ratio and C_H. However, only the HE model can quantitatively describe the deposition condition dependence of the H bonding structures.

(3) It was suggested that the random H-elimination (RHE) can cause selective monohydride formation in comparison with the CRN model.

ACKNOWLEDGMENTS

The authors thank Akiko Tabata, Mio Saito, Akira Mikami, Sigeki Matsuda, and Hiroshi Nonoue for their experimental assistance and advice in the composition analysis and IR measurement. The authors also wish to thank Norihiro Terada and Dr. Shingo Okamoto for their critical reading of this article. A part of this work was carried out at the New Materials Research Center of Sanyo Electric Co., Ltd., and was supported in part by the New Energy and Industrial Technology Development Organization as a part of the New Sunshine Program under the Ministry of International Trade and Industry.

*Electronic address: akira_terakawa@rd.sanyo.co.jp

[1] A. Terakawa, M. Shima, T. Kinoshita, M. Isomura, M. Tanaka, S. Kiyama, S. Tsuda, and H. Matsunami, Proceedings of the 14th EU Photovoltaic Solar Energy Conference, Barcelona, 1997 (unpublished), p. 2359.
[2] G. Lucovsky, R. J. Nemanich, and J. C. Knights, Phys. Rev. B **19**, 2064 (1979).
[3] C. J. Fung, K. J. Grunts, L. Ley, M. Cardona, F. J. Demond, G. Muller, and S. Kalbitzer, J. Non-Cryst. Solids **35&36**, 255 (1980).
[4] A. H. Mahan, P. Raboisson, and R. Tsu, Appl. Phys. Lett. **50**, 335 (1987).
[5] N. Nakamura, T. Takahama, M. Isomura, M. Nishikuni, K. Yoshida, S. Tsuda, S. Nakano, M. Ohnishi, and Y. Kuwano, Jpn. J. Appl. Phys. **28**, 1762 (1989).
[6] Y. Hishikawa, S. Tsuda, K. Wakisaka, and Y. Kuwano, J. Appl. Phys. **73**, 4227 (1993).
[7] Y. Hishikawa, K. Ninomiya, E. Maruyama, S. Kuroda, A. Terakawa, K. Sayama, H. Tarui, M. Sasaki, S. Tsuda, and S. Nakano, Proceedings of the 1st World Conference on the Photovoltaic Energy Conversion, Waikoloa, 1994, p. 386.
[8] S. Okamoto, Y. Hishikawa, S. Tsuge, M. Sasaki, K. Ninomiya, M. Nishikuni, and S. Tsuda, Jpn. J. Appl. Phys. **33**, 1773 (1994).
[9] A. Terakawa, M. Shima, K. Sayama, H. Tarui, H. Nishiwaki, and S. Tsuda, Jpn. J. Appl. Phys. **34**, 1741 (1995).
[10] S. Okamoto, Y. Hishikawa, and S. Tsuda, Jpn. J. Appl. Phys. **35**, 26 (1996).
[11] G. Lucovsky and G. N. Parsons, Optoelectron., Devices Technol. **4**, 119 (1989).
[12] F. Finger, V. Viret, A. Shah, X.-M. Tang, J. Weber, and W. Beyer, Mater. Res. Soc. Symp. Proc. **192**, 583 (1990).
[13] A. A. Langford, M. L. Fleet, P. B. Nelson, W. A. Lanford, and N. Maley, Phys. Rev. B **45**, 13 367 (1992).
[14] F. Gaspari, S. K. O'Leary, S. Zukotynski, and J. M. Perz, J. Non-Cryst. Solids **155**, 149 (1993).
[15] G. Ganguly and A. Matsuda, Phys. Rev. B **47**, 3661 (1993).
[16] K. Maeda, A. Kuroe, and I. Umezu, Phys. Rev. B **51**, 10 635 (1995).
[17] K. Sato, Y. Sugiyama, A. Uchiyama, S. Iwabuchi, T. Hirano, and H. Koinuma, Phys. Rev. B **46**, 1913 (1992).
[18] K. Sato, H. Hanna, S. Iwabuchi, T. Hirano, and H. Koinuma, Phys. Rev. B **50**, 2675 (1994).
[19] K. Nakajima, K. Miyazaki, H. Koinuma, and K. Sato, J. Appl. Phys. **84**, 606 (1998).
[20] E. Srinivasan, H. Yang, and G. N. Parsons, J. Chem. Phys. **105**, 5467 (1996).
[21] A. Terakawa and H. Matsunami, Jpn. J. Appl. Phys. **38**, 6207 (1999).
[22] D. E. Polk, J. Non-Cryst. Solids **5**, 365 (1971).
[23] A. Matsuda and K. Tanaka, J. Appl. Phys. **60**, 2351 (1986).